Exchange Factor Model for Radiative Heat Transfer Analysis in Rocket Engines

K. J. Hammad* and M. H. N. Naraghi†
Manhattan College, Riverdale, New York 10471

Numerical models based on the discrete exchange factor (DEF) and the zonal methods for radiative analysis of rocket engines containing a gray radiatively participating medium have been developed. These models implement a new technique for calculating the direct exchange factors to account for possible blockage by the nozzle throat. Given the gas and surface temperature distributions, engine geometry, and radiative properties, the models compute the wall radiative heat fluxes at different axial positions. The results of sample calculations for a typical rocket engine (engine 700 at NASA), which uses RP-1 (a kerosene-type propellant), are presented for a wide range of surface and gas properties. It is found that heat transfer by radiation can reach up to 50% of that due to convection. The maximum radiative heat flux is at the inner side of the engine, where the gas temperature is the highest. Although the results of both models are in excellent agreement, the computation time of the DEF method is found to be much smaller. Dimensionless radiative heat fluxes were calculated via a nonhomogeneous medium model using the DEF method.

Nomenclature

A_i	= area of surface zone i
DG_iG_j, DG_iS_j, $\overline{DS_iG_j}$, $\overline{DS_iS_j}$	= total exchange factors between differential gases and/or surfaces
$\overline{dg_ig_j}$, $\overline{dg_is_j}$, $\overline{ds_ig_j}$, $\overline{ds_is_j}$,	= direct exchange factors between differential gases and/or surfaces
E_i	= emissive power of surface or gas zone i
$\overline{G_iG_j}$, $\overline{G_iS_j}$, $\overline{S_iG_j}$, S_iS_j	= total exchange areas in the zone method
$\overline{g_ig_j}$, $\overline{g_is_j}$, $\overline{s_ig_j}$, $\overline{s_is_j}$	= direct exchange areas in the zone method
K_a	= absorption coefficient
K_s	= scattering coefficient
K_t	= extinction coefficient
N_g	= number of gas zones
N_s	= number of surface zones
q_s''	= surface heat flux
R	= radius of chamber and nozzle
r	= radial coordinate
r_{ij}	= distance between two points i and j
V_i	= volume of gas zone i
w	= numerical integration weight factor
z	= axial coordinate
α	= absorptivity
β_i	= angle between a vector normal to dA_i and axial direction
ε	= emissivity
θ_i	= angle between normal to dA_i and connecting line between i and j
ρ	= reflectivity
σ	= Stefan Boltzman constant
$\tau(r_{ij})$	= transmittance along path r_{ij}
ϕ	= angular coordinate
ω_o	= K_s/K_t, scattering albedo

Subscripts

g	= gas
i, j, k	= ith, jth, and kth surface or gas element
l	= lower limit of integration
s	= designates surface
u	= upper limit of integration

Received June 23, 1989; revision received June 8, 1990; accepted for publication June 12, 1990.

*Graduate Assistant, Department of Mechanical Engineering.
†Associate Professor, Department of Mechanical Engineering. Member AIAA.

Introduction

IN high-pressure spacecraft engines, such as SSME (Space Shuttle Main Engine), CTV (Chemical Transfer Vehicle), and HLLV (Heavy Lift Launch Vehicle), combustion products can reach very high temperatures, and radiation becomes a significant mode of heat transfer. The existing thermal model for rocket engines[1] considers convection as the only mode of heat transfer between combustion products, the thrust chamber, and nozzle walls. Two difficulties are involved in incorporating radiation into the analysis: the nonlinearity of the radiation terms, and the fact that radiative heat can travel long distances from one side of the engine to the other via multiple reflections and scattering from the surfaces and combustion products. Also, the complex configuration of the rocket engine, in particular, the blockage due to the throat, introduces more complexity into the analysis.

The existing model for radiative analysis of rocket engines assumes a transparent propellant.[2,3] This assumption is good for nuclear rockets or when hydrogen is used as a propellant. However, it is not a valid assumption for hydrocarbon propellants, in which the combustion products act as an absorbing-emitting and scattering medium. Howell et al.[4-7] used the Monte Carlo method to evaluate wall heat flux in a rocket engine containing hot gases, taking into account gas nonhomogeneity. In these works, however, the effects of surface reflection and surface emission were not considered.

The objective of this work is to present a model for radiative analysis of rocket engines. This model is based on the discrete exchange factor (DEF) method.[8-10] The DEF method is derived by discretizing the integral equations of the continuous exchange factor (CEF) method, using a numerical quadrature scheme. It has been shown that the DEF method provides accurate results for one-dimensional,[8] two-dimensional,[9] and three-dimensional[10] radiative transfer problems.

The zonal method[11-13] is also used to calculate the surface heat flux in the rocket engine. It should be noted that in the DEF method the direct exchange factors are between two

differential volumes and/or surfaces. Evaluating these exchange factors requires fewer integrations and less computational effort than evaluating those of the zonal method.

The major difficulty in evaluating direct exchange factors in both the DEF and the zonal methods is caused by the blockage at the throat area. This problem has been addressed by Robbins et al.[2,3] and Eddy and Nielsson[14] for the case of nonparticipating medium. The methods presented in these references cannot be used here because the medium is not transparent and view factors (direct exchange factors) are between gases and/or surfaces. In previous works,[2,3,14] it has been shown that the visible portion of a section of engine from the other side of the throat has a circular shape. This is true as long as the throat is sharply edged. In most nozzles, however, the throat has a smooth curvature; it will be shown that the visible part from the other side of the throat has an irregular shape.

Analysis

Consider the rocket thrust chamber and nozzle shown in Fig. 1. In the present analysis, the derivations are performed based on a gray gas model. The gray assumption is valid only in cases where the spectral properties of combustion gases are combined with those of the combustion generated particles (mainly soot). The detailed spectral properties of combustion gases will be suppressed when they are combined with those of the particles. Because of this, use of very accurate spectral properties of gases will result in a marginal enhancement in the accuracy of the analysis, but would definitely increase the computational time by some orders of magnitude. For nongray cases, however, a multiband model can be implemented to include the effect of spectral gas properties. The chamber walls are gray and diffuse surfaces. The chamber and nozzle are subdivided into a number of differential surface and differential gas zones in the DEF method (Fig. 1a), and into a number of surface and gas zones in the zonal method (Fig. 1b). The exit of the engine is assumed to be a black surface at the exit gas temperature; the surface at the left-hand side of the engine is considered to be at the same temperature as the first surface segment. In the following two sections, formulations based on the DEF and the zonal methods are presented.

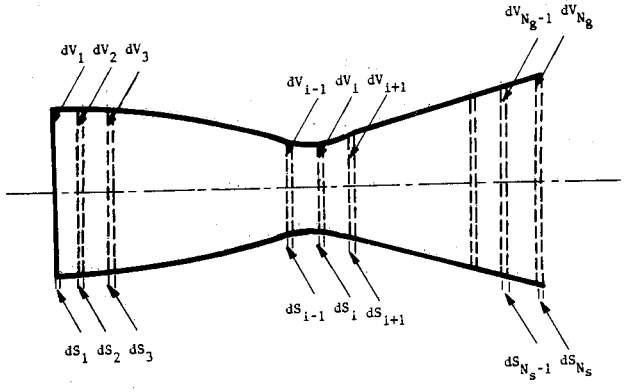

a) Differential surface and differential gas zones (DEF method)

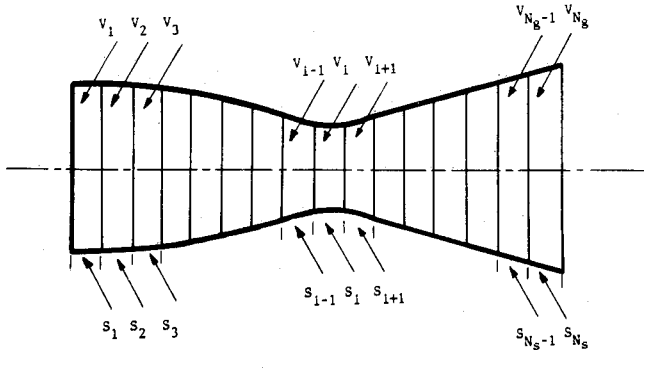

b) Surface and gas zones (zone method)

Fig. 1 Schematic of a rocket nozzle.

DEF Method Formulation

Based on the DEF method, the discrete direct exchange factors $\overline{ds_i s_j}$, $\overline{ds_i g_j}$, $\overline{dg_i s_j}$, and $\overline{dg_i g_j}$, are defined as the differential fraction of radiative energy that is emitted from a differential surface or gas at location i and reaches another differential surface or gas at location j by direct radiation.[8] The direct exchange factors between two differential surfaces and/or volumes are given by the following equations[15] (see Fig. 2 for notations):

$$\overline{ds_i s_j} = \frac{R_j}{2\pi^2}\int_{\phi_i}\int_{\phi_{jl}}^{\phi_{ju}} \frac{\cos\theta_i \cos\theta_j \tau(r_{ij})}{r_{ij}^2 \sin\beta_j}\, d\phi_j\, d\phi_i\, dz_j \quad (1)$$

$$\overline{ds_i g_j} = \frac{K_{tj}}{2\pi^2}\int_{\phi_i}\int_{\phi_{jl}}^{\phi_{ju}}\int_{r_{jl}}^{r_{ju}} \frac{r_j \cos\theta_i \tau(r_{ij})}{r_{ij}^2}\, dr_j\, d\phi_j\, d\phi_i\, dz_j \quad (2)$$

$$\overline{dg_i s_j} = \frac{R_j}{4\pi^2 R_i^2}\int_{r_i}\int_{\phi_i}\int_{\phi_{jl}}^{\phi_{ju}} \frac{r_i \cos\theta_j \tau(r_{ij})}{r_{ij}^2 \sin\beta_j}\, dr_i\, d\phi_j\, d\phi_i\, dz_j \quad (3)$$

and

$$\overline{dg_i g_j} = \frac{K_{tj}}{4\pi^2 R_i^2}\int_{r_i}\int_{\phi_i}\int_{\phi_{jl}}^{\phi_{ju}}\int_{r_i}\int_{r_{jl}}^{r_{ju}} \frac{r_i r_j \tau}{r_{ij}^2}(r_{ij})\, dr_j\, d\phi_j\, d\phi_i\, dr_i\, k\dot{z}_j \quad (4)$$

where

$$\cos\theta_i = \frac{r_i - r_j\cos(\phi_j - \phi_i) + (z_i - z_j)\dfrac{\partial f(z_i)}{\partial z}}{\left[1 + \left(\dfrac{\partial f(z_i)}{\partial z}\right)^2\right]^{1/2} r_{ij}}$$

$$\sin\beta_j = \left\{1 - \left\{\left(\frac{\partial f(z_j)}{\partial z}\right)^2 \Big/ \left[1 + \left(\frac{\partial f(z_j)}{\partial z}\right)^2\right]\right\}\right\}^{1/2}$$

$$r_{ij} = [r_i^2 + r_j^2 - 2r_i r_j \cos(\phi_j - \phi_i) + (z_i - z_j)^2]^{1/2}$$

and

$$\tau(r_{ij}) = e^{-\int_{r_i}^{r_j} K_t dr}$$

If the throat does not block the view of one section to another, the limits of integration ϕ_{jl}, ϕ_{ju}, r_{jl}, and r_{ju} are 0, 2π, 0, and R_j, respectively. If there is blockage, however, the integration limits are dependent upon the nozzle shape [i.e., the limits depend on the fraction of the differential volume/gas at location j that is visible to a point at location i (points C, D, and E in Fig. 3a)]. Let (r_i, ϕ_i, z_i) be coordinates of a typical point at section i, and (r_k, ϕ_k, z_k) coordinates of tangent points on the nozzle (e.g., point F in Fig. 3a). The dot product of unit vectors $\hat{\imath}$ and $\hat{n}$ yields

$$\phi_k = \phi_i + \cos^{-1}\left\{\frac{1}{r_i}\left[f(z_k) - \frac{\partial f(z_k)}{\partial z}(z_i - z_k)\right]\right\} \quad (5)$$

The argument of $\cos^{-1}$ in this equation must be in the range of $[-1, +1]$, requiring z_k to satisfy the condition

$$\left| f(z_k) - \frac{\partial f(z_k)}{\partial z}(z_i - z_k) \right| \leq r_i \quad (6)$$

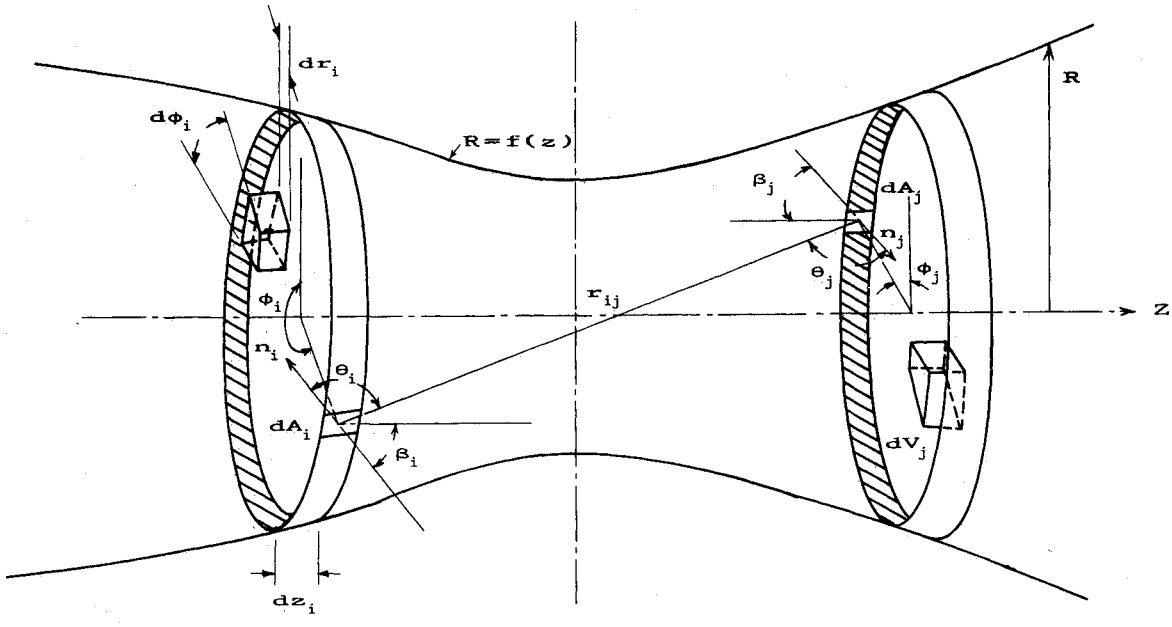

Fig. 2 Schematic of a typical differential surface and gas elements.

When point (r_i, ϕ_i, z_i) is at the centerline (e.g., point E in Fig. 3a), $r_i = 0$ and inequality (6) reduces to

$$f(z_k) - \frac{\partial f(z_k)}{\partial z}(z_i - z_k) = 0 \tag{7}$$

so that the tangent points on the throat are on the contour of a disk perpendicular to the axis of symmetry at z_k. When point (r_i, ϕ_i, z_i) is not at the centerline (e.g., points C or D), an iterative technique is used to estimate the range of z_k that satisfies inequality (6). The contour of the visible portion at section j [points (r_j, ϕ_j, z_j)] can be obtained by intersecting lines connecting (r_i, ϕ_i, z_i) and (r_k, ϕ_k, z_k) with the plane perpendicular to the axial direction at z_j. The resulting ϕ_j and r_j then become

$$\phi_j = \tan^{-1}\left[\frac{r_i \sin\phi_i + h(r_k \sin\phi_k - r_i \sin\phi_i)}{r_i \cos\phi_i + h(r_k \cos\phi_k - r_i \cos\phi_i)}\right]$$

$$r_j = \frac{1}{\sin\phi_j}[r_i \sin\phi_i + h(r_k \sin\phi_k - r_i \sin\phi_i)]$$

where

$$h = \frac{z_j - z_i}{z_k - z_i}$$

Typical visible portions of sections A-A and B-B from points C, D, and E are shown in Fig. 3. As mentioned in Ref. 14, the visibility of a finite narrow ring element A_j to a differential element dA_i can be restricted because of three factors. The first is the blocking by an intermediate segment (addressed also by Robbins[2]). The second is blocking by the horizon (when the angle between the local normal to dA_i and the line connecting dA_i and dA_j is greater than $\pi/2$). Finally the third, which is blocking due to orientation of A_j (when the angle between the line connecting dA_i and dA_j and the local normal to dA_j is greater than $\pi/2$). Eddy and Nielsson also provided expressions for calculating the visible portion (angle ϕ) of a narrow ring element A_j when viewed from a differential element dA_i. The minimum ϕ for various types of blocking was used as the circumferential limit of integration when calculating radiation shape factors for channels with varying cross sections. In the process of evaluating ϕ, they assumed that the width of the ring element is small, Δz, such that no visibility restrictions appear when integrating over Δz. Eddy and Nielsson[14] approximated the visible portion as a circle. This approximation is good in the present application only when the emitting point i is close to the centerline, but introduces significant error when emitting points are located away from the centerline.

Once the contour of the visible portion is determined, the limits of integration in Eqs. (1–4) (i.e., ϕ_{jl}, ϕ_{ju}, r_{jl}, and r_{ju}) can be evaluated. The value of r_{jl} for the cases shown in Fig. 3b is 0. When the visible portion falls below the centerline, r_{jl} is the shortest distance (at angle ϕ_j) between the centerline and the visible area. The value of r_{ju} is the largest distance between the visible portion and the centerline (at the same angle ϕ_j). Upper and lower limits of angle ϕ_j for the gas section are its highest and lowest values at the visible area, respectively. For the surface, however, these limits are the angles of intersecting points of the visible area contour and surface of the nozzle. The surface is invisible when the contour is within the boundaries of the section.

Since the rocket nozzle has an axisymmetric configuration, it is easier to perform calculations for blockage treatment in the cylindrical coordinate system. For more general cases, however, it may be preferable to use the Cartesian coordinates system, where the equation of a ray emitted from point (x_i, y_i, z_i) and tangent to the surface at point (x_k, y_k, z_k) requires the solution of the quadratic equation

$$Ax_k^2 + Bx_k + C = 0 \tag{8}$$

where

$$A = \frac{x_i^2}{y_i^2} + 1$$

$$B = -2f(z_k)\left[f(z_k) + \frac{\partial f(z_k)}{\partial z}(z_i - z_k)\right]\frac{x_i}{y_i^2}$$

and

$$C = \frac{f(z_k)x_i}{y_i^4}\left[f(z_k) + \frac{\partial f(z_k)}{\partial z}(z_i - z_k)\right]^2 - f^2(z_k)$$

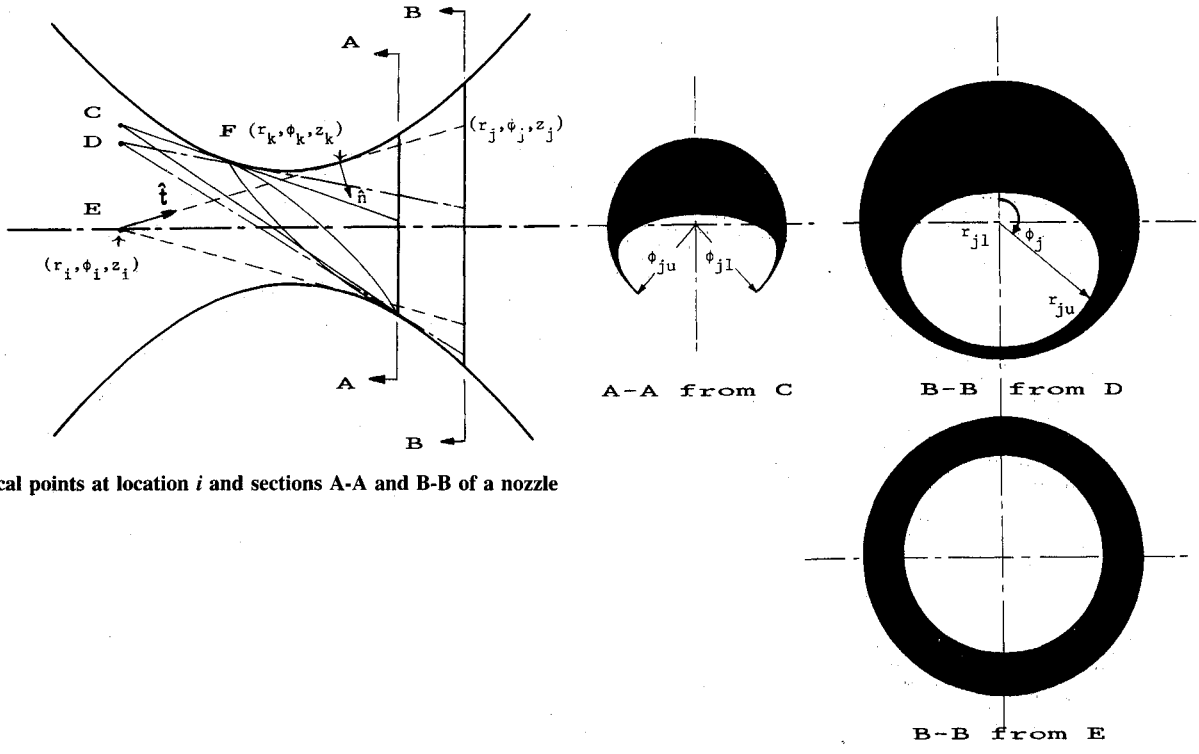

a) Typical points at location i and sections A-A and B-B of a nozzle

b) Visible portions of sections A-A and B-B from Points C, D, and E

Fig. 3 Blockage due to the throat.

Note, values of z_k in this equation must satisfy

$$B^2 - 4AC \geq 0 \tag{9}$$

Once x_k and z_k are determined, y_k is calculated using the function generator of the nozzle surface via the following equation:

$$x_k^2 + y_k^2 = f^2(z_k) \tag{10}$$

The point of intersection of the ray with a section perpendicular to the axial direction at z_j is determined using

$$x_j = x_i + (z_j - z_i)\frac{(x_k - x_i)}{(z_k - z_i)}$$

$$y_j = y_i + (z_j - z_i)\frac{(y_k - y_i)}{(z_k - z_i)}$$

The exchange factors calculated from Eqs. (1–4) must satisfy the conservation of energy equations. The discretized forms of these equations are given by[8]

$$\sum_{j=1}^{N_s} w_{s_j}\overline{ds_i s_j} + \sum_{j=1}^{N_g} w_{g_j}\overline{ds_i g_j} = 1 \tag{11}$$

and

$$\sum_{j=1}^{N_s} w_{s_j}\overline{dg_i s_j} + \sum_{j=1}^{N_g} w_{g_j}\overline{dg_i g_j} = 1 \tag{12}$$

These equations imply that the radiative energy emitted from a surface or volume node will reach another surface or volume node within the enclosure. The direct exchange factors calculated from Eqs. (1–4) do not necessarily satisfy conservation equations (11–12), since Eqs. (1–4) are solved numerically. This is also encountered in the zonal method. (Techniques to normalize exchange factors were reported in Refs. 16–18.) In calculating the direct exchange factors between coincident elements ($z_i = z_j$), r_{ij} in Eqs. (1–4) becomes very small or zero, causing singularity at these elements. To overcome the singularity, Gaussian quadrature methods with different orders at element i than those at element j are used.

Once the discrete direct exchange factors are determined, the discrete total exchange factors can be evaluated using explicit matrix formulations presented in Ref. 8. The discrete total exchange factor between two differential elements $\overline{DZ_i Z_j}$ is the fraction of energy that is emitted from a differential surface or gas at i, and reaches another differential surface or gas at j by direct radiation and multiple reflection and scattering from surfaces and gas, respectively. Like the direct exchange factors, there are also four total exchange factors: $\overline{DS_i S_j}$, $\overline{DS_i G_j}$, $\overline{DG_i S_j}$, and $\overline{DG_i G_j}$, and they satisfy conservation of energy equations.

After calculating the discrete total exchange factors, the heat flux and emissive powers of the surface can be related via

$$q''_{s_i} = \frac{\sin\beta_i}{2\pi R_i}\left(E_{s_i} - \sum_{j=1}^{N_s} w_{s_j}E_{s_j}\overline{DS_j S_i} - \sum_{j=1}^{N_g} w_{g_j}E_{g_j}\overline{DG_j S_i}\right) \tag{13}$$

where

$$E_{s_i} = \varepsilon_i\sigma\frac{2\pi R_i}{\sin\beta_i}T_{s_i}^4$$

and

$$E_{g_j} = 4K_{ij}(1 - \omega_o)\sigma\pi R_j^2 T_{g_j}^4$$

are surface and gas zone emissive powers, respectively. The weight factors w_s and w_g are used for numerical integration along the axial direction. Their values are given by $\{\Delta z/2, \Delta z,$

$\Delta z, \ldots, \Delta z, \Delta z/2\}$ and $\{\Delta z/3, 4\Delta z/3, 2\Delta z/3, \ldots, 2\Delta z/3, 4\Delta z/3, \Delta z/3\}$ for trapezoidal and Simpson's methods, respectively. Note that $\Delta z = L/(n-1)$, where L is the length of engine and n is the number of discrete points along axial direction.

Zonal Method Formulation

In the zonal method, the direct exchange areas $\overline{z_i z_j}$ ($\overline{s_i s_j}$, $\overline{s_i g_j}$, $\overline{g_i s_j}$, and $\overline{g_i g_j}$) are defined as the portion of radiative energy that is emitted from zone z_i and reaches zone z_j by direct radiation. The direct exchange areas have dimensions of area and are given by[15]

$$\overline{s_i s_j} = 2\pi \int_{z_{i-1}}^{z_i} \int_{z_{j-1}}^{z_j} R_i \overline{ds_i s_j}\, dz_i \tag{14}$$

$$\overline{s_i g_j} = 2\pi \int_{z_{i-1}}^{z_i} \int_{z_{j-1}}^{z_j} R_i \overline{ds_i g_j}\, dz_i \tag{15}$$

$$\overline{g_i s_j} = 4\pi \int_{z_{i-1}}^{z_i} \int_{z_{j-1}}^{z_j} K_t R_i^2 \overline{dg_i s_j}\, dz_i \tag{16}$$

and

$$\overline{g_i g_j} = 4\pi \int_{z_{i-1}}^{z_i} \int_{z_{j-1}}^{z_j} K_t R_i^2 \overline{dg_i g_j}\, dz_i \tag{17}$$

Note that the evaluation of direct exchange areas of the zonal method require two more integrations than that of the DEF method for the present one-dimensional application. Provided the medium is gray, the direct exchange areas obey reciprocity, and energy conservation requires that

$$\sum_{j=1}^{N_s} \overline{s_i s_j} + \sum_{j=1}^{N_g} \overline{s_i g_j} = A_i \tag{18}$$

and

$$\sum_{j=1}^{N_s} \overline{g_i s_j} + \sum_{j=1}^{N_g} \overline{g_i g_j} = 4K_{t_i} V_i \tag{19}$$

where

$$A_i = \pi(R_i + R_{i-1})\left[(z_i - z_{i-1})^2 + (R_i - R_{i-1})^2\right]^{1/2}$$

and

$$V_i = \frac{\pi}{3}(z_i - z_{i-1})\left[R_i^2 + 2R_i R_{i-1} + R_{i-1}^2\right]$$

Similar to the DEF method, the direct exchange areas calculated from Eqs. (14–17) do not necessarily satisfy the above equations. The same procedure that was used in the DEF method is used to reinforce the conservation equations (18) and (19).

In the zonal method, the dimensional total exchange area $\overline{Z_i Z_j}$ ($\overline{S_i S_j}$, $\overline{S_i G_j}$, $\overline{G_i S_j}$, and $\overline{G_i G_j}$) is the ratio of the radiation energy emitted from zone z_i, which is absorbed by zone z_j (directly or after reflection and/or scattering from other zones) to the total hemispherical emissive power of zone z_i. The unified matrix formulation given in Ref. 19 is used to evaluate the total exchange areas.

Once the total exchange areas are determined, the radiative heat flux to the surface zone s_i is calculated using the following equation:

$$q''_{s_i} = \varepsilon_i \sigma T_{s_i}^4 - \frac{1}{A_i}\left(\sum_{j=1}^{N_s} \sigma T_{s_j}^4 \overline{S_j S_i} + \sum_{j=1}^{N_g} \sigma T_{g_i}^4 \overline{G_j S_i}\right) \tag{20}$$

Results and Discussion

The numerical models introduced in the previous section are used to determine the radiative heat flux at the inner surface of a rocket thrust chamber and nozzle. To study the effect of different gas and surface properties on the radiation heat flux, a rocket engine, namely, engine 700, is considered. This is a high-pressure booster rocket engine; its nozzle radius vs axial position is given in Table 1. This engine uses RP-1, which is a kerosene-type propellant, as fuel, and its oxidant is liquid oxygen. The surface and gas static temperatures at different axial positions in the engine are determined using the rocket thermal evaluation code[20] and combustion code.[21] The resulting surface and gas temperatures at different engine axial positions for chamber stagnation pressure of 1200 psi are given in Table 2.

To implement the numerical model, the tabular values of the nozzle diameters are curve fitted into an algebraic expression using least square curve fitting. A 25th order polynomial, whose coefficients are found in Table 3, is found to be the best fit for the given engine geometry. To avoid inaccurate results, the curve fitting computation must be performed in a double precision format. A piecewise curve fitting may be used to obtain lower order polynomials. The combustion process produces combustion gases, such as water vapor, carbon dioxide, carbon monoxide, and others. These gases don't scatter radiation significantly, but are strong absorbers and emitters of radiant energy. Only liquid droplets in the early stages of combustion and combustion-generated particles are the major contributors to radiation scattering among the combustion product species. The combustion gas species mole fractions are obtained from the combustion code[21] containing 17% CO_2, 30% CO, 33% H_2O, 6% OH, 2.5% O_2, 3% H, 7% H_2, 1.5% O. The equilibrium combustion code[21] greatly underestimates the formation of particles (soot). A more realistic prediction or experimental measurement of the volume fractions, sizes, shapes, and distribution of these particles along the rocket engine is necessary to include soot radiation in the present analysis. Since the objective of the current paper is to present a new model, the details of presenting results based on real radiative properties of the combustion

Table 1 Nozzle radii along axial axis, in.

i	z_i	R_i	i	z_i	R_i
1	7.000	3.130	30	−2.106	1.714
2	6.380	2.959	31	−2.306	1.758
3	5.024	2.600	32	−2.506	1.799
4	3.500	2.191	33	−2.706	1.843
5	2.000	1.790	34	−2.906	1.885
6	1.200	1.575	35	−3.106	1.928
7	1.000	1.521	36	−3.306	1.970
8	0.500	1.389	37	−3.506	2.011
9	0.337	1.344	38	−3.706	2.050
10	0.287	1.334	39	−3.906	2.085
11	0.237	1.321	40	−4.106	2.120
12	0.187	1.315	41	−4.306	2.150
13	0.137	1.310	42	−4.506	2.180
14	0.087	1.305	43	−4.706	2.208
15	0.037	1.302	44	−4.906	2.234
16	0.000	1.300	45	−5.106	2.260
17	−0.050	1.302	46	−5.306	2.281
18	−0.100	1.305	47	−5.506	2.300
19	−0.150	1.310	48	−5.706	2.318
20	−0.200	1.316	49	−5.906	2.333
21	−0.274	1.328	50	−6.106	2.348
22	−0.506	1.374	51	−6.306	2.360
23	−0.706	1.418	52	−6.506	2.370
24	−0.906	1.462	53	−6.706	2.380
25	−1.106	1.503	54	−6.906	2.387
26	−1.306	1.546	55	−7.106	2.391
27	−1.506	1.586	56	−7.306	2.395
28	−1.706	1.630	57	−7.572	2.400
29	−1.906	1.672			

Table 2 Surface and gas temperatures along axial axis

i	z_i	T_{si}, °R	T_{gi}, °R
1	−7.572	1250.0	6708.6
2	−6.843	1244.4	6708.3
3	−6.115	1237.1	6707.5
4	−5.386	1222.0	6706.0
5	−4.658	1208.8	6703.6
6	−3.929	1205.1	6699.9
7	−3.200	1131.2	6692.6
8	−2.472	1062.9	6680.2
9	−1.743	1078.1	6660.8
10	−1.015	1106.5	6621.9
11	−0.286	1105.8	6509.7
12	0.443	908.8	6150.6
13	1.171	896.8	5885.3
14	1.900	926.0	5692.7
15	2.628	871.3	5549.5
16	3.357	803.3	5415.1
17	4.086	736.2	5306.3
18	4.814	669.3	5203.9
19	5.543	579.1	5116.1
20	6.271	479.6	5034.3
21	7.000	380.0	4952.5

Table 3 Polynomial coefficients for nozzle function generator

n	a_n
1	1.30726493130758
2	1.03197893262880E-02
3	2.68201115774000E-01
4	1.59380493498145E-02
5	−9.41218459080475E-02
6	−7.83976187762828E-03
7	2.33987586202858E-02
8	2.09780098773611E-03
9	−3.56903698798999E-03
10	−3.34936431843993E-04
11	3.48788379508638E-04
12	3.39705538673131E-05
13	−2.26731304789299E-05
14	−2.27698235505887E-06
15	1.00074491870502E-06
16	1.03100878456710E-07
17	−3.00977088742926E-08
18	−3.16884055658690E-09
19	6.07043667147034E-10
20	6.51308731982046E-11
21	−7.85250352024550E-12
22	−8.56763853404065E-13
23	5.88574281855297E-14
24	6.51995292960792E-15
25	−1.94313794828692E-16
26	−2.18268086878700E-17

products is left for future reports. The handbook of infrared radiation from combustion gases[22] is used to obtain the gas absorption coefficient K_a. The properties reported in this handbook are spectral and temperature-dependent. Hence, an integrated averaged value for the absorption coefficient is calculated, and is found to be $K_a = 2.5$ in.$^{-1}$ This value was obtained by integrating the spectral or band absorption coefficients from a narrow band model[22] over the entire spectrum for the given composition, temperatures, and at atmospheric pressure. To examine the effect of absorption coefficient and scattering albedo on the wall heat flux, the results for different values of K_a (varying from optically thin to optically thick) and ω_o are presented.

A comparison between the results of the DEF method and the zonal method, when $\varepsilon = 0.95$ and chamber pressure is 1200 psi for different absorption coefficient values, is presented in Fig. 4. As shown in this figure, the agreement between the results of DEF method and those of zone method is excellent. Figure 4 also demonstrates the effect of the propellant absorption coefficient. The peak heat flux increases with K_a, due to the increase in the emissive power and absorption in the optically thick propellant, which traps energy in the converging part of the nozzle and prevents it from escaping downstream the nozzle. The heat flux variation in the nozzle shows a different pattern for optically thin gases. Figure 5 shows a comparison between the radiative and convective (1 and 20) heat fluxes when the gas is nonscattering and $K_a = 2.5$ in.$^{-1}$. These results indicate that the convective heat flux is consistently greater than the radiative flux, contrary to the results presented by Howell et al.,[4-7] where a nuclear rocket engine with a hydrogen propellant was investigated (using gas temperatures, approximately twice as large as those for hydrocarbon fuels in the present analysis). Also, note that the nuclear rockets studied in Refs. 4–7 are radiatively cooled, whereas the engine investigated in this work is regeneratively cooled via channels along its walls. And it should be noted that the maximum convective heat flux is near the

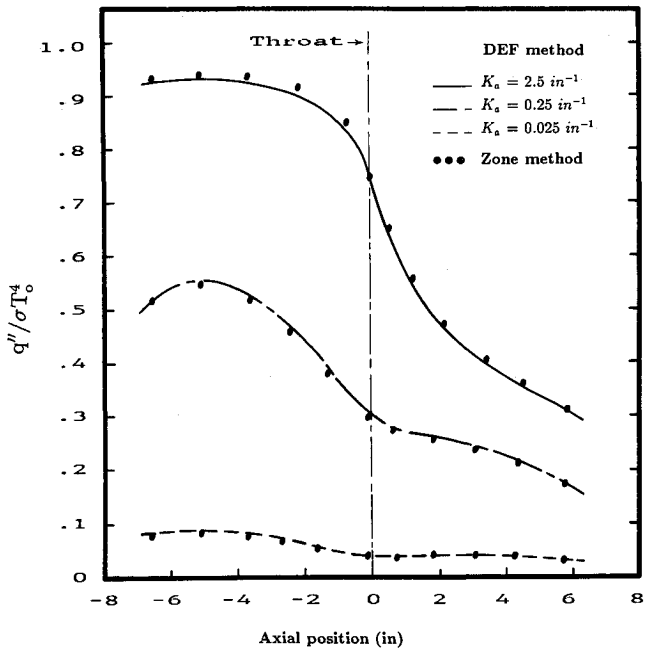

Fig. 4 Effect of absorption coefficient on dimensionless radiative heat fluxes based on both the zone and the DEF methods.

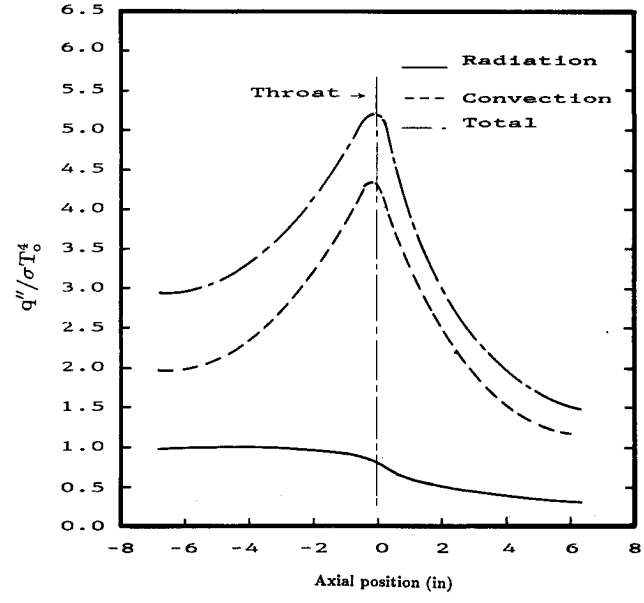

Fig. 5 Dimensionless convective and radiative surface heat fluxes at $K_t = 2.5$ in.$^{-1}$ and = 1.

throat, whereas the largest radiation flux is close to the engine inlet.

The effect of scattering albedo on the surface heat flux is shown in Fig. 6. The gas extinction coefficient is 2.5 in.$^{-1}$, and the heat flux distribution for all scattering albedo shows the same trend. Figure 7 shows the effect of surface emissivity. As expected, the radiative heat flux increases with surface emissivity. Although the radiative flux can be substantially reduced by using highly reflective surfaces, carbon deposits on the walls from combustion products (raising the surface emissivity to a value of about 0.9) negate this effect after the first few seconds of engine operation.

To demonstrate the effect of gas nonhomogeneity, the values of K_t were assumed to vary with gas temperature and pressure according to the correlation $K_t = (aT_{g_s} + b)P_{g_s}^m$, where $a = 0.0002135$, $b = -0.9326$, and $m = 0.1$. This correlation and the constants a, b, and m were chosen to give a rough estimation of the variation of K_t with gas temperature and pressure; however, a more accurate evaluation of K_t as a function of combustion gases temperatures, pressures, and composition is required to demonstrate the actual variation of radiative heat flux with gas nonhomogeneity. Since K_t values increase with gas pressure and temperature, the highest value of K_t was chosen to be at the inner side of engine chamber, while the lowest value is at the nozzle exit. As shown in Fig. 8, the peak heat flux increased in the converging part of the nozzle and a more rapid decrease in the heat flux occurred in the throat area for the case of a nonhomogeneous gas, whereas lower values of heat flux in the diverging part of the nozzle are predicted in comparison with the case of the homogeneous gas, at $K_t = 0.25$ in.$^{-1}$.

Finally, the dimensionless radiative heat flux distribution

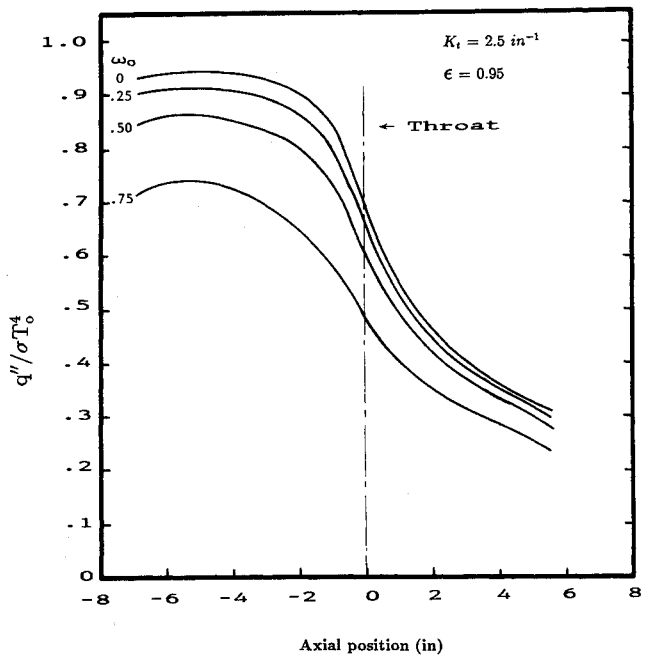

Fig. 6 Effect of propellant scattering albedo on dimensionless radiative heat fluxes at K_t = 2.5 in.$^{-1}$ and = 0.95.

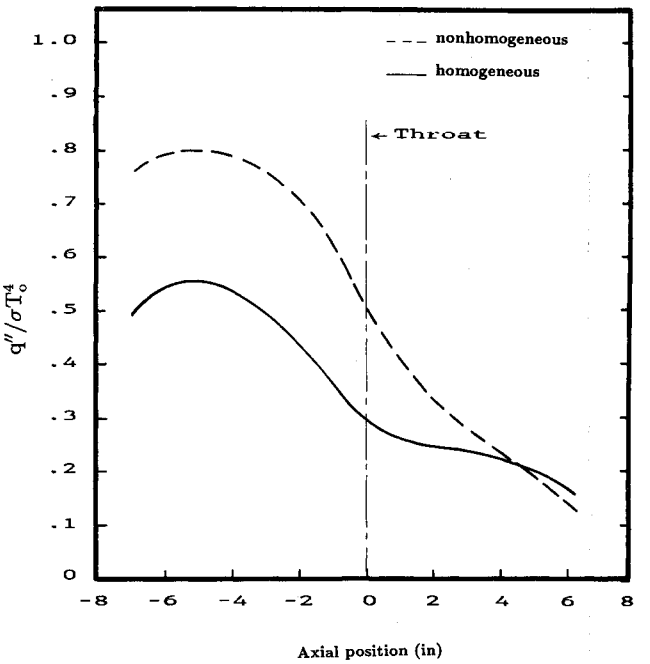

Fig. 8 Effect of gas nonhomogeneity on dimensionless radiative heat fluxes.

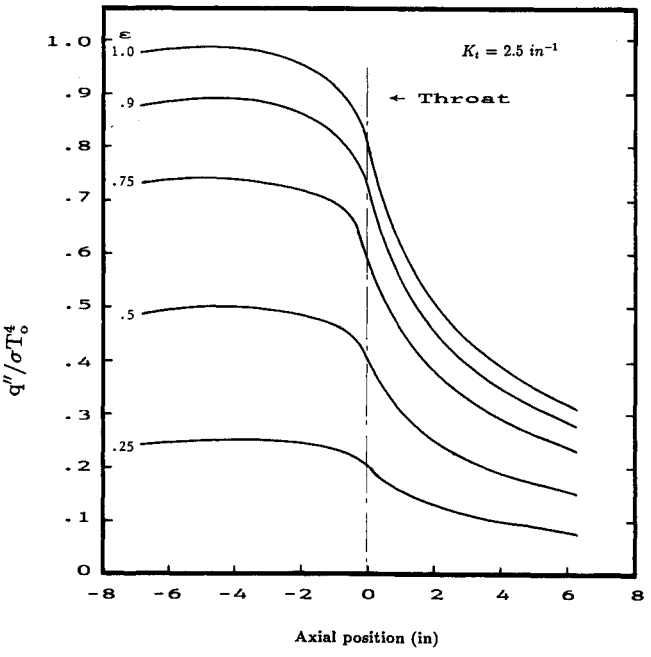

Fig. 7 Effect of surface emissivity on dimensionless radiative heat fluxes at K_t = 2.5 in.$^{-1}$

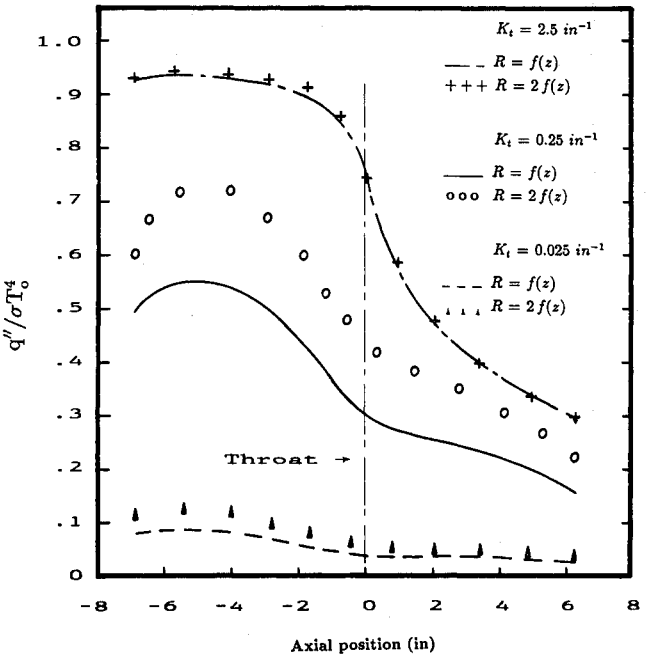

Fig. 9 Effect of engine size on dimensionless radiative heat fluxes at K_t = 2.5, 0.25, and 0.025 in.$^{-1}$

was calculated using values of nozzle diameters that are twice those listed in Table 1. A comparison between calculated heat fluxes when the engine size was doubled compared to those calculated earlier at values of K_t, which vary from optically thin to optically thick medium, is shown in Fig. 9. As expected, the effect of engine size variation on surface heat flux is very significant for optically thin gases, where an increase of up to 50% in surface heat flux values was obtained at $K_t = 0.025$ in.$^{-1}$. The effect of engine size on surface heat flux is not noticeable for optically thick gases, where a maximum increase of only 3% in surface heat flux was obtained at $K_t = 2.5$ in.$^{-1}$. This expected small increase for optically thick gases is due to the fact that the most significant contribution to the surface radiative heat flux comes from gas elements that are very close to the surface, and increasing engine size will have only marginal effect on surface heat flux. In contrast, for the case when the medium is optically thin, the radiation heat transfer from gas elements that are located far away from the surface contributes significantly to surface radiative heat flux.

Concluding Remarks

The DEF method was used to analyze the radiative heat transfer in rocket engines containing a radiatively participating medium, taking into account gas nonhomogeneity. The numerical results obtained are in excellent agreement with those of the zonal method. The computational time for the DEF method, however, is much less than that of the zonal method. The computational time for zonal method is approximately $2n$ times that of the DEF method, where n is the order of Gaussian quadrature method used for numerical integration in Eqs. (14–17).

A new technique to account for blockage by the throat in calculating the direct exchange factors is presented. It has been shown that the visible area of a section of engine from the other side of throat can have a noncircular configuration. This is contrary to the results in Refs. 2, 3, and 14, where a circular shape for the visible area is reported. Radiative heat fluxes to the surface increase significantly with engine size when the gas is optically thin, compared to a marginal increase in the case of optically thick gas. This is due to the fact that the most significant contribution to surface heat flux in optically thick medium comes from gas elements that are very close to the nozzle surface.

In this work, only gray radiation is considered. For nongray cases, a band model, in which the range of active wavelength is subdivided into finite bands, can be employed. At each band, nongray band properties are assumed; by integrating over all bands, the nongray solution can be obtained. The gas temperature and pressure vary along the axial direction, making the gas nonhomogeneous. The gas absorption factor as a function of temperature for some combustion species is presented in Ref. 22; however, the data for radiative properties of combustion gases as a function of pressure are incomplete. More research in evaluating spectral radiative properties of combustion gases based on different temperatures and pressures is needed for more accurate radiative analysis of rocket engines.

The existing combustion code for rockets[21] is capable of evaluating all thermodynamic and transport properties of combustion gas except radiative properties. This code needs to be modified to incorporate radiative properties of all combustion species. It should be emphasized that reliable results will be obtained only when accurate properties of the combustion products are used in the analysis.

The present paper and works by Robbins[2,3] and Howell et al.[4–7] clearly demonstrate that radiation is an important mode of heat transfer in rocket engines. More work in the radiation analysis of rocket engines is needed to incorporate the effects of spectral properties and anisotropic scattering into the existing model.

Acknowledgment

This work was supported by NASA, Lewis Research Center, under Grant NAG 3-892.

References

[1]Naraghi, M. H. N., and Armstrong, E. S., "Three Dimensional Thermal Analysis of Rocket Thrust Chambers," AIAA Paper 88-2643, AIAA Thermophysics, Plasmadynamics, and Lasers Conf., San Antonio, TX, June 27–29, 1988.

[2]Robbins, W. H., "An Analysis of Thermal Radiation Heat Transfer in a Nuclear-Rocket Nozzle," NASA TN D-586, January 1961.

[3]Robbins, W. H., and Todd, C. A., "Analysis, Feasibility, and Wall Temperature Distribution of a Radiation Cooled Nuclear Rocket Nozzle," NASA TN D-878, January 1962.

[4]Howell, J. R., Strite, M. K., and Renkel, H., "Heat Transfer Analysis of Rocket Nozzles Using Very High Temperature Propellants," *AIAA Journal*, Vol. 3, No. 4, 1965.

[5]Howell, J. R., and Strite, M. K., "Heat Transfer in Rocket Nozzles Using High-Temperature Hydrogen Propellants with Real Property Variations," *Journal of Spacecraft and Rockets*, Vol. 3, No. 7, 1966.

[6]Howell, J. R., and Renkel, H., "Analysis of the Effect of a Seeded Propellant Layer on Thermal Radiation in the Nozzle of a Gaseous-Core Nuclear Propulsion System," NASA TND-3119, 1965.

[7]Howell, J. R., Strite, M. K., and Renkel, H., "Analysis of Heat Transfer Effects in Rocket Nozzles Operating with Very High-Temperature Hydrogen," NASA TR R-220, 1965.

[8]Naraghi, M. H. N., Chung, B. T. F., and Litkouhi, B., "A Continuous Exchange Factor in Enclosures with Participating Media," *Journal of Heat Transfer*, Vol. 110, No. 2, 1988, pp. 456–462.

[9]Naraghi, M. H. N., and Kassemi, M., "Radiative Heat Transfer in Rectangular Enclosures: A Discretized Exchange Factor Solution," *ASME Proceedings of the 1988 National Heat Transfer Conference*, Edited by H. R. Jacobs, Vol. 1, American Society of Mechanical Engineering, New York, pp. 259–267; also Journal of Heat Transfer, Vol. 111, No. 4, 1988, pp. 1117–1119.

[10]Naraghi, M. H. N., and Litkouhi, B., "Discrete Exchange Factor Solution of Radiative Heat Transfer in Three-Dimensional Enclosures," Presented at the National Heat Transfer Conf., Philadelphia, PA, August 6–9, 1989.

[11]Hottel, H. C., and Cohen, E. S., "Radiation Heat Exchange in a Gas-filled Enclosure; Allowance of Non-uniformity of Gas Temperature," *AIChE Journal*, Vol. 4, No. 1, 1958, pp. 3–14.

[12]Hottel, H. C., and Sarofim, A. F., "Gaseous Radiation with Temperature Gradient Allowance for Isotropic Satter," *Research in Heat Transfer*, 1963, pp. 139–150.

[13]Hottel, H. C., and Sarofim, A. F., *Radiative Transfer*, McGraw-Hill, NY, 1967.

[14]Eddy, T. L., and Nielsson, G. E., "Radiation Shape Factors for Channel with Varying Cross Section," *Journal of Heat Transfer*, Vol. 110, No. 1, 1988, pp. 264–266.

[15]Hammad, K. J., "Radiative Heat Transfer Analysis in Rocket Thrust Chambers and Nozzles," M. S. Thesis, Dept. of Mechanical Engineering, Manhattan College, Riverdale, NY, 1989.

[16]Sowell, E. F., and O'Brien, P. F., "Efficient Computation of Radiant-Interchange Configuration Factors Within the Enclosures," *Journal of Heat Transfer*, Vol. 94, No. 3, 1972, pp. 326–328.

[17]Vercammen, H. A. J., and Forment, G. F., "An Improved Zone Method Using Monte Carlo Techniques for the Simulation of Radiation in Industrial Furnaces," *International Journal of Heat and Mass Transfer*, Vol. 23, No. 3, 1980, pp. 329–336.

[18]Larsen, M. E., and Howell, J. R., "Least-squares Smoothing of Direct-exchange Areas in Zonal Analysis," *Journal of Heat Transfer*, Vol. 108, No. 1, 1986, pp. 239–242.

[19]Naraghi, M. H. N., and Chung, B. T. F., "A Unified Matrix Formulation for the Zone Method: A Stochastic Approach," *International Journal of Heat and Mass Transfer*, Vol. 28, No. 1, 1986, pp. 245–251.

[20]Naraghi, M. H. N., "RTE-A Computer Code for Three Dimensional Rocket Thermal Evaluation," Manhattan College Rept., Riverdale, NY, prepared for NASA Lewis Research Center, Grant No. NAG 3-759, 1988.

[21]Gordon, S., and McBride, B. J., "Computer Program for Calculation of Complex Chemical Equilibrium Compositions, Rocket Performance, Incident and Reflection Shocks, and Chapman-Jouquet Detonations," NASA SP-273, 1971.

[22]Ludwig, C. B., Malkmus, W., Reardon, J. E., and Thomson, J. A. L., "Handbook of Infrared Radiation From Combustion Gases," NASA SP-3080, 1973.